SUPPLEMENTARY INFORMATION

doi:10.1038/nature11574

A. A theoretical framework to calculate climate sensitivity.

B. Details on data for temperature changes ΔT and radiative forcing changes ΔR, from which climate sensitivity is calculated, for the three examples:

   B.1 the late Pleistocene (last 800 ka),

   B.2 the mid-Pliocene (3 Ma),

   B.3 the Eocene-Oligocene transition (35 Ma), and

   B.4 the PETM (56 Ma).

C. The application of the theoretical framework described in A to the example of the late Pleistocene including a comparison of three different approaches to calculate climate sensitivity.

A. Theoretical framework for climate sensitivity

We describe in the following a consistent framework how to calculate climate sensitvity based on palaeo data. We distinguish between fast and slow feedbacks and how this might be calculated from data. We derive the equations from the basis up, for clarity, and to illustrate how the entire framework discussed in this study is consistent throughout. Components of this follow similar procedures that were either implicitly or explicitly developed in previous studies, often from the theory of feedback analysis[1,2].

a. The problem

For determining present-day climate sensitivity, we are interested in the global mean temperature response ΔT due to changes in greenhouse gas concentrations (in particular CO_2) over a time scale τ. The change of CO_2 causes a change in radiative heat flux $\Delta R_{[\mathrm{CO_2}]}$ which will lead to a response in the climate system giving additional radiative heat fluxes $\Delta R_{[P]}$ due to processes labelled here in an abstract way with a subscript P. Each of these radiative heat fluxes will contribute to the global temperature increase ΔT.

The additional radiative heat fluxes $\Delta R_{[P]}$ will not all change at the same time scale as τ. Some will arise much faster than τ and some will appear at a much longer time scale than τ. So we can naturally group the processes P into two categories: the fast processes P^f with time scales smaller than τ and the slow processes P^s with time scales larger than τ. The radiative heat flux changes due to the slow processes P^s have no effect on ΔT on the time scale τ and hence only the fast processes contribute to the radiative heat flux changes responsible for ΔT. This forms the basis for the definition of the equilibrium or Charney[3] climate sensitivity where τ is chosen as 100 year. We denote the Charney climate sensitivity as S^a (where the superscript a refers to actuo) and it is given by

$$S^a = \frac{\Delta T}{\Delta R_{[\mathrm{CO_2}]}}, \tag{1}$$

where the total response ΔT (due to all fast processes with respect to the time scale τ) is measured with respect to the radiative heat flux change due to the change in atmospheric CO_2.

Each radiative heat flux $\Delta R_{[P]}$ due to a process P contributes to the temperature change and

hence it is useful to define a specific climate sensitivity $S_{[P]}$ as

$$S_{[P]} = \frac{\Delta T}{\Delta R_{[P]}}. \tag{2}$$

In this way, we see from (1) that the Charney climate sensitivity S^a can be expressed as

$$S^a = S_{[\mathrm{CO_2}]}. \tag{3}$$

When we want to combine the effect of two different processes P_1 and P_2, it is useful to define a specific climate sensitivity $S_{[P_1,P_2]}$ as

$$S_{[P_1,P_2]} = \frac{\Delta T}{\Delta R_{[P_1]} + \Delta R_{[P_2]}}. \tag{4}$$

The problem addressed in the main paper is how to estimate values of S^a from proxy data such as changes in temperature and CO_2 concentrations during glacial-interglacial cycles. These changes occur over much longer time scales than τ and hence also slow processes P^s contribute to the changes in ΔT. In extreme cases only estimates of specific sensitivities $S_{[P^s]}$ may be available. The main question addressed here is how to estimate values of S^a from these data.

b. An illustrative conceptual model

To illustrate how S^a can be computed from proxy data, we use a conceptual model of the Earth system representing processes determining the surface temperature T, the land-ice extent L and the atmospheric carbon content (below indicated by C) relative to a reference value, say C_0. The global mean temperature T is governed by the energy balance model equation

$$c_T \frac{dT}{dt} = Q(1 - \alpha(T, L)) + A(T) \ln C - \sigma \epsilon T^4, \tag{5}$$

where c_T is the thermal inertia (in J $(\mathrm{m^2K})^{-1}$). The first term in the right hand side models the short-wave radiation with Q (in $\mathrm{Wm^{-2}}$) being the solar constant divided by four and α the planetary albedo. For reasons of simplicity albedo here in this conceptual model is restricted to temperature dependent sea-ice processes. The term $A(T) \ln C$ (in $\mathrm{Wm^{-2}}$) models the effect of greenhouse gases on the radiation balance, where the function $A(T)$ includes a representation of water vapour processes. Finally the last term in Eq. (5) models the long-wave radiation with σ ($\mathrm{Wm^{-2}K^{-4}}$) being the Stefan-Boltzmann constant and ϵ the emissivity.

The models for L (land ice) and C (atmospheric carbon content) are only given schematically by

$$\frac{dL}{dt} = \frac{1}{\tau_L} f_L(T, L, t), \tag{6a}$$

$$\frac{dC}{dt} = \frac{1}{\tau_C} f_C(T, C, t) + \frac{1}{\tau_f} F_C(t), \tag{6b}$$

where τ_L is a typical time scale of land-ice changes modelled by processes represented in f_L. The latter function includes the net effect of Milankovitch orbital forcing on the land-ice extent. Similarly, τ_C is the typical time scale of changes in atmospheric CO_2 concentration due to natural carbon cycle processes (e.g. volcanoes, weathering) that are represented by f_C. The term $F_C(t)$ represents the human induced CO_2 emissions (including fast responses, such as those of the biosphere) which occur on the time scale τ_f.

We will now determine specific climate sensitivities for (i) the present-day case and for (ii) a typical paleoclimate case, i.e., the glacial-interglacial transitions.

(i) The present-day case

For the present-day case, the forcing time scale τ_f is taken as 100 years (doubling of CO_2) and the time scales τ_L and τ_C are much longer ($>$ 1000 years). So if we are interested in the sensitivity of the temperature due to changes in CO_2 on a time scale $\tau = \tau_f$, we effectively have

$$\frac{dL}{dt} \approx 0, \tag{7a}$$

$$\frac{dC}{dt} \approx \frac{1}{\tau_f} F_C(t). \tag{7b}$$

Indeed on the time scale τ the ice extent will not change much, and neither will natural carbon cycle processes affect CO_2 levels. When the emission function $F_C(t)$ is given, the solution for $C(t)$ follows directly from Eq. (7b). As C is then independent of temperature, it acts as a *forcing* in Eq. (5) and as L does not change, α in Eq. (5) is effectively only a function of T.

For example, when an emission function is chosen to illustrate the phasing out of fossils fuels (Supplementary Fig. 1) as

$$F_C(t) = \frac{C_2 - C_1}{\cosh^2 \frac{t}{\tau_f}}, \tag{8}$$

the solution $C(t)$ is

$$C(t) = C_1 + (C_2 - C_1)\tanh(\frac{t}{\tau_f}). \tag{9}$$

This indicates an increasing value of C, starting at C_1 for $t = 0$ and equilibrating on a time scale τ_f to a new value C_2.

Suppose first that the water-vapour processes do not change much over the temperature range considered and hence A can be assumed to be constant. The radiative heat flux due to greenhouse gases, $A \ln C$, is clearly a function of time but it also equilibrates quickly for times larger than τ_f and the change on a time scale τ_f is given by $\Delta R_{[\mathrm{CO_2}]} = A \ln C_2/C_1$. Let T_1 and T_2 be the equilibrium temperatures under the concentrations C_1 and C_2, respectively. From Eq. (5), the difference $\Delta T = T_2 - T_1$ is determined by the equations

$$0 = Q(1 - \alpha(T_1)) + A \ln C_1 - \sigma\epsilon T_1^4, \tag{10a}$$

$$0 = Q(1 - \alpha(T_2)) + A \ln C_2 - \sigma\epsilon T_2^4, \tag{10b}$$

By subtracting both equations it is found that

$$A \ln C_2/C_1 = \sigma\epsilon(T_2^4 - T_1^4) + Q(\alpha(T_2) - \alpha(T_1)), \tag{11}$$

and when ΔT is small with respect to T_1 we can expand

$$T_2^4 - T_1^4 \approx 4T_1^3\Delta T, \tag{12a}$$

$$\alpha(T_2) \approx \alpha(T_1) + \Delta T\alpha'(T_1), \tag{12b}$$

where the prime indicates differentiation to T. Now define the radiative flux due to outgoing long wave (OLW) radiation as $\Delta R_{[OLW]} = -4\sigma\epsilon T_1^3\Delta T$ and that due to sea-ice (SI) albedo changes as $\Delta R_{[SI]} = -Q\alpha'(T_1)\Delta T$ then it follows from Eq. (11) that

$$\Delta R_{[\mathrm{CO_2}]} = A \ln C_2/C_1 = -\Delta R_{[OLW]} - \Delta R_{[SI]}. \tag{13}$$

The Charney climate sensitivity S^a is then given by

$$S^a = S_{[\mathrm{CO_2}]} = \frac{\Delta T}{\Delta R_{[\mathrm{CO_2}]}} = \frac{-\Delta T}{\Delta R_{[OLW]} + \Delta R_{[SI]}}, \tag{14}$$

where the equality follows from the surface energy balance (13). One can also divide by ΔT to give

$$S^a = \frac{-\Delta T}{\Delta R_{[OLW]} + \Delta R_{[SI]}} = \frac{-1}{\lambda_P + \lambda_\alpha}, \tag{15}$$

where the first factor $\lambda_P = \Delta R_{[OLW]}/\Delta T = -4\sigma\epsilon T_1^3$ is the Planck feedback parameter and the second term $\lambda_\alpha = \Delta R_{[SI]}/\Delta T = -Q\alpha'(T_1)$ represents the albedo-sea-ice feedback parameter (or any other fast feedback process affecting the albedo) referenced at the temperature T_1. The sign of the λ is chosen such that a negative (positive) value will lead to a decreasing (increasing) Charney sensitivity[4]. In particular, the Planck feedback parameter λ_P is negative and the albedo-sea-ice feedback parameter λ_α is positive. Note that the associated surface heat fluxes are in the right hand side of the balance (13).

When $A(T)$ does vary over the temperature range $[T_1, T_2]$, then the equilibrium temperatures are found from

$$0 = Q(1-\alpha(T_1)) + A(T_1)\ln C_1 - \sigma\epsilon T_1^4, \tag{16a}$$

$$0 = Q(1-\alpha(T_2)) + A(T_2)\ln C_2 - \sigma\epsilon T_2^4. \tag{16b}$$

With $\Delta R_{[\mathrm{CO_2}]} = A(T_1)\ln C_2/C_1$ and the same approximations (and $A(T_2) \approx A(T_1) + A'(T_1)\Delta T$) we find

$$S^a = \frac{-\Delta T}{\Delta R_{[OLW]} + \Delta R_{[SI]} + \Delta R_{[WV]}}, \tag{17}$$

where $\Delta R_{[WV]} = \Delta T\ A'(T_1)\ln C_2$ is the radiative flux change due to water vapour processes. With λ_A being the water vapour feedback parameter, the expression above for S^a can be written as

$$S^a = \frac{-1}{\lambda_P + \lambda_\alpha + \lambda_A}. \tag{18}$$

By including an arbitrary number N of fast processes in addition to the Planck feedback, Eq. (18) generalizes to

$$S^a = \frac{-1}{\lambda_P + \sum_{i=1}^{N}\lambda_i^f}, \tag{19}$$

with again $\lambda_P < 0$, which is equation (1) in the main text.

For the present-day case, the situation is very clear with respect to forcing and feedbacks. Due to the difference in time scales between the change in CO_2 due to human emissions and the natural processes giving rise to land-ice and carbon dioxide changes, the greenhouse gas increase acts as a forcing and the other processes (water - vapour, Planck and sea-ice) act as feedbacks. In Eq. (13), we have therefore written the forcing on the left hand side of the surface energy balance and the feedbacks on the right hand side.

(ii) Glacial-Interglacial transitions

We now consider the glacial cycle variations within the same conceptual model with climate variations on a time scale of at least 10,000 year. The external forcing of the system is the Milankovitch forcing of which the annual mean component is very small; only the average response due to internal processes in the climate system is presented in our conceptual model. With $F_C = 0$, the equations (6) for the land-ice extent L and the CO_2 concentration C become

$$\frac{dL}{dt} = \frac{1}{\tau_L} f_L(T, L, t), \tag{20a}$$

$$\frac{dC}{dt} = \frac{1}{\tau_C} f_C(T, C, t). \tag{20b}$$

The characteristic time of adjustment of the global mean temperature is much smaller then τ_L and τ_C and hence T is always in equilibrium with the slow changes in the climate system, i.e.,

$$0 = Q(1 - \alpha(T, L)) + A \ln C - \sigma \epsilon T^4, \tag{21}$$

where A is (only for simplicity) considered to be constant. Over a long time interval, the land-ice extent and CO_2 concentration change, say from L_1 to L_2 and from C_1 to C_2, respectively. The temperature difference is now determined by

$$0 = Q(1 - \alpha(T_1, L_1)) + A \ln C_1 - \sigma \epsilon T_1^4, \tag{22a}$$

$$0 = Q(1 - \alpha(T_2, L_2)) + A \ln C_2 - \sigma \epsilon T_2^4. \tag{22b}$$

The radiative heat flux due to CO_2 changes is again directly given by $\Delta R_{[CO_2]} = A \ln C_2/C_1$ similar to that in the present-day case for constant A. However, in the albedo we now have terms from both the sea-ice and the land-ice changes giving

$$\alpha(T_2, L_2) - \alpha(T_1, L_1) \approx (\frac{\partial \alpha}{\partial T}(T_1) + \frac{\partial \alpha}{\partial L}\frac{\partial L}{\partial T}(T_1))\Delta T. \tag{23}$$

Subtracting Eq. (22a) from Eq. (22b) now gives

$$A \ln C_2/C_1 - Q\frac{\partial \alpha}{\partial L}\frac{\partial L}{\partial T}(T_1)\Delta T = Q\frac{\partial \alpha}{\partial T}(T_1)\Delta T + 4\sigma \epsilon T_1^3 \Delta T. \tag{24}$$

We define $\Delta R_{[LI]} = -Q\frac{\partial \alpha}{\partial L}\frac{\partial L}{\partial T}(T_1)\Delta T$ and hence we can write the Eq. (24) above as

$$\Delta R_{[CO_2]} + \Delta R_{[LI]} = -\Delta R_{[SI]} - \Delta R_{[OLW]}. \tag{25}$$

Note that we put the surface heat flux $\Delta R_{[LI]}$ in the left hand side of the balance (25) as we consider it a forcing which is needed to account for the effect of the slow feedback on the total temperature change. At this point, there are several choices to define the paleoclimate sensitivity. As in most cases, only data on CO_2 and ΔT is available, a direct choice is to define S^p analogous to S^a as $S^p = S_{[\mathrm{CO}_2]}$. We will refer to S^p as the Earth System sensitivity. In this case, from the conceptual model, we find directly that

$$S^p = S_{[\mathrm{CO}_2]} = \frac{\Delta T}{\Delta R_{[\mathrm{CO}_2]}} = \frac{-\Delta T}{\Delta R_{[OLW]} + \Delta R_{[SI]} + \Delta R_{[LI]}} = \\ = \frac{-1}{\lambda_P + \lambda_\alpha + \lambda_L}, \tag{26}$$

where we define $\lambda_L = \Delta R_{[LI]}/\Delta T$. Compared to Eq. (15), we get an extra feedback term ($\lambda_L = \Delta R_{[LI]}/\Delta T = -Q\frac{\partial \alpha}{\partial L}\frac{\partial L}{\partial T}(T_1)$) due to albedo effects of the land-ice changes. Again a positive (negative) sign of the slow feedback parameter λ_L indicates an increase (decrease) in Earth System sensitivity.

c. How to calculate S^a from S^p?

From the conceptual model and under the assumptions of small ΔT (with respect to T_1) one can easily find S^a from S^p from the relation

$$S^a = S^p(1 + \frac{\lambda_L}{\lambda_P + \lambda_\alpha}), \tag{27}$$

which indicates that a positive value of λ_L (assuming $\lambda_P + \lambda_\alpha < 0$) and will lead to $S^a < S^p$. Hence, we have 'corrected' S^p for the slow feedback process to provide the Charney climate sensitivity S^a.

The equation (27) generalizes to (cf. equation (2) in the main text)

$$S^a = S^p(1 + \frac{\sum_{j=1}^{M} \lambda_j^s}{\lambda_P + \sum_{i=1}^{N} \lambda_i^f}), \tag{28}$$

where each $\lambda_j^s = \Delta R_{[P_j^s]}/\Delta T$ represents the feedback parameters of each slow process P_j^s.

Eq. (28) implies that we would need to know the strengths of the heat fluxes of both the fast and slow feedbacks. However, there are easier ways to determine S^a from proxy data when assumptions are made on the surface energy balance. From the surface energy balance in the

conceptual model Eq. (25), we see that S^a can be computed from the specific climate sensitivity $S_{[\mathrm{CO}_2,LI]}$ since

$$S_{[\mathrm{CO}_2,LI]} = \frac{\Delta T}{\Delta R_{[\mathrm{CO}_2]} + \Delta R_{[LI]}} = \frac{-\Delta T}{\Delta R_{[SI]} + \Delta R_{[OLW]}} = S^a. \tag{29}$$

So by treating the radiation changes due to land-ice changes as a *forcing* in the climate sensitivity (and hence on the left hand side of the surface energy balance), an approximation of the relevant S^a is obtained without the need to know all feedback parameters. This holds under the assumption on the form of the (linearized) surface energy balance which is in equilibrium during glacial-interglacial transitions. An example can be found in Hansen and Sato[5], where from records of temperature, atmospheric CO_2 concentration and land-ice changes, the Charney sensitivity is estimated from $\Delta R_{[\mathrm{CO}_2]}$ and $\Delta R_{[LI]}$.

This can be generalized to include more slow feedback processes. In the surface energy balance, we put all slow processes (with respect to the 100 year time scale) on the left hand side and all fast ones in the right hand side. We then compute the specific climate sensitivity

$$S_{[\mathrm{CO}_2,P_1^s,\cdots,P_m^s]} = \frac{\Delta T}{\Delta R_{[\mathrm{CO}_2]} + \sum_{j=1}^{m} \Delta R_{[P_j^s]}}, \tag{30}$$

and due to (linearized) surface energy balance, we find (if in reality there are M slow processes) that

$$S^a = \lim_{m \to M} S_{[\mathrm{CO}_2,P_1^s,\cdots,P_m^s]}. \tag{31}$$

In several model studies of palaeoclimates, the starting point is a model configuration of a present-day state (say pre-industrial) and then the background situation is changed towards the appropriate configuration of the past. For example, the land-ice distribution is adapted, a different vegetation distribution is applied, the CO_2 concentration is changed and the appropriate orography is implemented. When an equilibrium solution of this climate model under the 'best' configuration is determined, then a temperature difference ΔT (with respect to the present-day configuration) is determined and the Earth system sensitivity S^p can be directly calculated from ΔT and $\Delta R_{[\mathrm{CO}_2]}$. Numerical experiments can also be done in a stepwise manner, i.e. first the land-ice is added and an equilibrium state is computed; next the CO_2 concentration is changed and a new equilibrium is computed. For each step, a temperature difference can be calculated.

The notation of climate sensitivity introduced here can very well be used in results from GCM simulations. Note that we have basically three types of climate sensitivity: S^a (Charney) is reserved for the response of the present-day state to CO_2 increase over a time scale of 100 year, S^p (Earth System sensitivity) is reserved for general climate change involving changes in CO_2 but where ΔT is also due to processes on a longer time scale than 100 year. For all other cases, we can use the specific climate sensitivities $S_{[X,Y,...]}$.

For example, using a double CO_2 experiment under present-day conditions where slow feedbacks do not play any role, one will determine directly S^a, but when a different climate background state is used, one finds $S_{[CO_2]}$. If slow feedbacks play a role, one finds S^p. Note that in the latter case, one needs to determine $S_{[CO_2,LI,...]}$ to approximate S^a from S^p (just like from observations as above).

As another example, for a simulation in which CO_2 is fixed but the land-ice configuration is changed, the surface heat flux balance will include fast and slow feedback terms, but no $R_{[CO_2]}$. Hence from such a simulation, one can only determine the specific climate sensitivity $S_{[LI]}$. There is no CO_2 subscript and as consequence, $S_{[LI]}$ cannot be directly used in the approximation of S^a. An additional GCM simulation with varying CO_2 concentration is needed to accomplish this.

B. Calculation of climate sensitivity based on proxy data

Based on palaeoclimate data we may calculate several specific climate sensitivities and the Earth system sensitivity S^p and from these estimate the Charney climate sensitivity S^a. By doing so we have to realise the following caveats:

- Effects of changes in the reference temperature T_1. It may well be that the fast feedbacks like sea-ice and cloud feedbacks depend on the reference temperature[6–8]. For example, it could be that sea-ice is much more sensitive to temperature changes under cold conditions than under warm conditions.
- Effects of linearisation. The error due to the linear approximations in ΔT, as are for example made in Eq. (12), should be small, i. e., ΔT should be small compared to T_1.
- Effects of changes of the slow feedbacks. This is particularly important if the specific climate sensitivities are to be used for a range of values of the carbon dioxide concentration, which are not overlapping with the range used to derive the specific climate sensitivity.
- Transient effects. Climate sensitivity as discussed here is restricted to equilibrium climate sensitivity. Because we cannot be certain that the underlying data sets are restricted to equilibrium climate states, restrictions on the data used may have to be introduced.

B.1 The Pleistocene Having noted the above limitations we can calculate the specific climate sensitivities $S_{[X]} = \Delta T/\Delta R_{[X]}$ based on different explicitly considered processes X.

We based our temperature anomaly on a model-based deconvolution[9] of the benthic δ^{18}O stack LR04[10] into sea level and temperature. This approach calculates surface air temperature in high northern latitudes ΔT_{NH} $(40-80^\circ$ N) (Supplementary Fig. 2A), from which we calculate the global temperature anomaly ΔT (Supplementary Fig. 2B) as follows:

$$\Delta T = \frac{\Delta T_{NH}}{a}. \tag{32}$$

Here, a polar amplification factor on northern high latitude land area $a = 2.75 \pm 0.25$ $(\pm 1\sigma)$ is used. This leads to ΔT at LGM (23 –19 ka BP) of -5.1 K to -6.1 K, in good agreement with the

-5.8 ± 1.4 K, found by Schneider von Deimling et al. [11]. This extrapolates proxy-based evidences on local temperature anomalies by means of a climate model to the global scale. Furthermore, a agrees with other estimates on high northern polar amplification[12]. Note, that the uncertainty in the deconvolution of the temperature anomaly contributes most to the uncertainty in ΔT, while the uncertainty in a is only of minor importance. For example, the relative uncertainty in ΔT at the LGM is 18%, to which the uncertainty in ΔT_{NH} contributes 16%.

The red dotted line (Supplementary Fig. 2B) indicates the threshold of $\Delta T = -1.5$ K below which ΔT needs to fall to permit robust calculations on climate sensitivity, otherwise high variability would be achieved. This is required because the temperature record[9] is not very reliable if there is nearly no ice in North America and Eurasia as the present-day ice sheets in Greenland and Antarctica are not explicitly accounted for.

All calculations of S are performed on the datasets of radiative forcing over the last 800 ka as compiled by Köhler et al.[4]. The two extreme examples are given in Supplementary Fig. 3. Either only CO_2 is given as radiative forcing ($\Delta R_{[CO_2]}$), or all available radiative forcings (CO_2, CH_4, N_2O (all three also grouped together as greenhouse gases GHG), albedo changes caused by land ice sheets, sea ice, vegetation and dust/aerosols) are added. All explicit effects of the slow feedbacks (forcings) X leading to different calculations of $S_{[X,Y,...]}$ compiled in Supplementary Table 1 may be looked up in detail in the source study. Note, that in the cases in which we consider changes in the surface albedo caused by the land-ice sheets LI (e.g. $S_{[X,LI,Y]}$) we do not consider all effects summed together previously[4] under *land cryosphere*. We only consider the effect of land ice sheets and sea level change, but not of snow cover change (which is a fast feedback). However, whether or not the effect of sea level change on surface albedo is considered might differ in other studies. This might be relevant if studies are compared as the sea level contribution to radiative forcing is at LGM, with nearly 20% of the pure land-ice sheet radiative forcing, not negligible. Grey bands give a $\pm 1\ \sigma_1$ uncertainty in Supplementary Fig. 3.

To avoid transient effects on climate sensitivity, we restrict the considered data sets to times, when global temperature change is either (a) < 0.5 K per kyr, or (b) < 0.1 K per kyr. Case (a) was chosen because it implies that all data points in the LGM ($19 - 23$ ka BP) are then considered to be in equilibrium, while case (b) was taken as a more strict criteria to avoid potential transient

climate states and their effects.

The mean specific climate sensitivity S is calculated by the arithmetic mean

$$S = \bar{S} = \frac{1}{K} \sum_{k=1}^{K} S_k, \tag{33}$$

where $S_k = S_{[X]}(t_k)$ is the specific climate sensitivity at time t_k. Thus, with $K = 8000$, k is running over the individual time steps that exist in the underlying data with $\Delta t = 100$ years. The calculated individual S_k for time step k is only considered as robust (and used for further analysis) when both conditions on temperature and radiative forcing anomaly are fulfilled:

$$\Delta T < -1.5 \text{ K and } \Delta R < -0.5 \text{ W m}^{-2}. \tag{34}$$

Both thresholds are indicated by red broken lines in Supplementary Figs. 2B and 3, in which the chosen time series of global temperature anomaly ΔT and radiative forcings ΔR are plotted. This filter procedure helps to extract large variability in S_k for small ΔT and ΔR, leading to the consideration of K' data points in the calculation of S, $K' < 8000$.

This dataset offers two alternatives for calculating the uncertainty in the mean specific climate sensitivity:

1. $\overline{\sigma_1}$: mean of the individual $\sigma_{1,k}$ uncertainties for all k considered time steps (grey band, Supplementary Fig. 4C, Fig. 5C, Fig. 6C) (K (W m^{-2})$^{-1}$). This error estimate follows the square root of the sum of squares, thus

$$\overline{\sigma_1} = \frac{1}{K'} \sum_{k=1}^{K'} \sigma_{1,k} \text{ with } \sigma_{1,k} = \sqrt{\sum_{j=1}^{M} \sigma_{k,j}^2}, \tag{35}$$

with j running over the M different processes contributing to S. In detail, this should be strictly followed only if the individual components contributing to S (thus to ΔT or ΔR) are independent, which is not always guaranteed. However, for reasons of simplicity we assume this independence is the case and a valid use of $\sigma_{1,k}$ is possible.

2. $\sigma_0(S)$: uncertainty of the averaging for (S) (K (W m^{-2})$^{-1}$):

$$\sigma_0(S) = \sqrt{\overline{S_k^2} - S^2} \text{ with } \overline{S_k^2} = \frac{1}{K'} \sum_{k=1}^{K'} S_k^2. \tag{36}$$

For small time windows (e.g. the LGM) $\sigma_0(S)$ is an order of magnitude smaller than $\overline{\sigma_1}$, while for longer periods (e.g. whole 800 kyr), $\sigma_0(S)$ increases significantly with respect to a smaller time window, while $\overline{\sigma_1}$ is roughly similar with respect to a smaller time window (Supplementary Table 1). This implies that using a larger dataset leads to larger uncertainties σ_0 in S, likely due to non-stationarity in the time series. The maximum of the calculated values σ_0 and $\overline{\sigma_1}$ should be taken as the uncertainty in the results. Note also, that S for the LGM are different from S derived from the 800 kyr sampling window, a fact which illustrates the state-dependency of S (Supplementary Table 1), which will be discussed in section C.

B.2 The Pliocene The mid-Pliocene ($\sim$ 3 to 3.3 Ma) is a period of well-documented warming relative to the Quaternary (last $\sim$ 2 million years), and is potentially useful for informing palaeosensitivity because the forcings which contributed to its warmth are relatively well understood. This period has previously been studied in this context [13], but here we present a new analysis that follows the framework proposed in this paper.

Initially, we assume that the fundamental 'external' forcings ($\Delta R_{[EXT]}$) which led to the mid-Pliocene warmth were (a) increased concentrations of atmospheric CO_2, ($\Delta R_{[CO_2]}$ [e.g. 14–16]) and (b) tectonic (orography) change ($\Delta R_{[OR]}$, primarily lower mid-Pliocene Rockies[17]). We assume that the CO_2 and orography forcings are independent (i.e. one is not a feedback to the other), that they add linearly, and assume that the Earth system responds with all other feedbacks (both 'fast' and 'slow'). The global mean temperature change is ΔT, so that, in the notation in this paper, the Earth system sensitivity

$$S^p = S_{[EXT]} = \frac{\Delta T}{\Delta R_{[EXT]}} = \frac{\Delta T}{\Delta R_{[CO_2]} + \Delta R_{[OR]}}. \tag{37}$$

Here ΔT can be estimated by considering a compilation of mid-Pliocene SST proxy estimates produced by the PRISM project [18]. Conversion of the SST estimates to the required global average near-surface air temperature is problematic, not least because of sparse and uneven data coverage, and the lack of direct proxy data over land or seaice regions. Several methods could be used; here we make use of existing model simulations of the mid-Pliocene, an approach also used recently[13]. A simulation of the mid-Pliocene, carried out using the HadCM3 model, gives reasonable agreement with the PRISM mid-Pliocene SST proxy dataset[19], and the simulated SST global mean is in good agreement with an interpolated version of the proxy dataset (mean SST difference of only 0.15 K). The mid-Pliocene was simulated in the model by implementing changes in the model to

the CO_2, orography, vegetation and land ice boundary conditions relative to pre-industrial[17]. These changes are based on observational datasets, such as pollen records[20] for the vegetation, and sea-level estimates from palaeo-shorelines[21] for ice sheets. This model gives a value of mid-Pliocene global mean near-surface air temperature increase relative to preindustrial, ΔT = 3.3 K, which can be used in Eq. (37).

$\Delta R_{[\mathrm{CO_2}]}$ is the radiative forcing of the CO_2, in this case assumed to be from 280 to 400 ppmv. Assuming a logarithmic dependence of CO_2 forcing on concentration, this is about half the forcing of that due to a CO_2-doubling, so $\sim 0.5 \cdot 3.7$ Wm^{-2} = 1.91 Wm^{-2}.

$\Delta R_{[OR]}$ in Eq. (37), the forcing due to changes in orography, can also be estimated from model simulations. In addition to mid-Pliocene and preindustrial simulations, Lunt et al. [22] carried out various sensitivity studies in which combinations of CO_2, orography, land ice, and vegetation boundary conditions were modified between preindustrial and Pliocene. These allow the global mean temperature change associated with these four boundary conditions, that is $\Delta T_{\mathrm{CO_2}}$, ΔT_{OR}, ΔT_{LI}, ΔT_{VG} respectively, to be estimated (see Lunt et al.[22] for more details). Assuming the CO_2 and orography forcings have the same efficacy as each other[23], then we can write $\Delta R_{[OR]}$ = $\Delta R_{[\mathrm{CO_2}]} \cdot \Delta T_{OR}/\Delta T_{\mathrm{CO_2}}$, so that

$$S^p = S_{[EXT]} = \frac{\Delta T}{\Delta R_{[\mathrm{CO_2}]}\left(1 + \frac{\Delta T_{OR}}{\Delta T_{\mathrm{CO_2}}}\right)} \tag{38}$$

The model sensitivity studies give $\Delta T_{\mathrm{CO_2}} = 1.6$ K and $\Delta T_{OR} = 0.7$ K, giving a value $S^p = S_{[EXT]}$ = 1.2 K(Wm^{-2})$^{-1}$. The Charney climate sensitivity can also be estimated directly from the model results (with only CO_2 varying) as

$$S^a = \frac{\Delta T_{\mathrm{CO_2}}}{\Delta R_{[\mathrm{CO_2}]}} = 0.82 \text{ K } (\text{W m}^{-2})^{-1}. \tag{39}$$

The model simulations also allow specific climate sensitivities S to be estimated. For example, if we consider the reduced Pliocene ice sheets as a forcing instead of as a feedback, we can calculate

$$S_{[EXT,LI]} = \frac{\Delta T}{\Delta R_{[\mathrm{CO_2}]} + \Delta R_{[OR]} + \Delta R_{[LI]}}. \tag{40}$$

With the same assumptions about efficacy, we can write $\Delta R_{[LI]} = \Delta R_{[\mathrm{CO_2}]} \cdot \Delta T_{LI}/\Delta T_{\mathrm{CO_2}}$ giving

$$S_{[EXT,LI]} = \frac{\Delta T}{\Delta R_{[\mathrm{CO_2}]}\left(1 + \frac{\Delta T_{OR}}{\Delta T_{\mathrm{CO_2}}} + \frac{\Delta T_{LI}}{\Delta T_{\mathrm{CO_2}}}\right)}. \tag{41}$$

The model sensitivity studies give ΔT_{LI} = 0.51 K, so $S_{[EXT,LI]}$ = 0.97 K $(\mathrm{Wm}^{-2})^{-1}$.

In a similar way for vegetation,

$$S_{[EXT,LI,VG]} = \frac{\Delta T}{\Delta R_{[\mathrm{CO}_2]}\left(1 + \frac{\Delta T_{OR}}{\Delta T_{\mathrm{CO}_2}} + \frac{\Delta T_{LI}}{\Delta T_{\mathrm{CO}_2}} + \frac{\Delta T_{VG}}{\Delta T_{\mathrm{CO}_2}}\right)}, \tag{42}$$

and ΔT_{VG} = 0.52 K, giving $S_{[EXT,LI,VG]}$ = 0.82 K $(\mathrm{Wm}^{-2})^{-1}$. This sensitivity is identical to the Charney sensitivity S^a in Eq. (39), as we have included all effects of the slow feedbacks (land ice and vegetation) as forcings.

There are several uncertainties associated with the estimate of the Pliocene sensitivity, which also apply to the work of Lunt et al. [13]. Firstly, we assume that the seasonal forcing due to orbital variability is zero. However, it could be that some of the imposed vegetation and ice sheet changes implemented in the model have a component that is due to orbital forcing, rather than solely CO_2 and orography forcing as is assumed here. If this were the case, S^p would be more similar to S^a (identical to S^a if all the vegetation and land ice changes were actually due to orbital forcing). Furthermore, there are uncertainties associated with the imposed forcings and feedbacks themselves. For example, more recent topographic reconstructions have suggested that the mid-Pliocene orography was actually more similar to modern than previously thought[24]. A model simulation carried out in the framework of the PlioMIP project[25] with HadCM3, which also includes more recent boundary conditions for vegetation and land ice, gives a value of ΔT = 3.3 K (which, by coincidence, is almost unchanged from the previous estimate). With $\Delta R_{[OR]} = 0$ in Eq. (37), this gives S^p = 1.73 K (Wm^{-2}). Also, there are likely to be feedbacks associated with the carbon cycle, such that some of the forcing included in $\Delta R_{[\mathrm{CO}_2]}$ is actually due to non-CO_2 greenhouse gas forcings. Assuming that warmer climates in general had higher non-CO_2 greenhouse gas concentrations (as is consistent with the Quaternary ice core record), this would result in a greater value of S^p, due to a lower value of $\Delta R_{[\mathrm{CO}_2]}$ in Eq. (37).

B.3 The Eocene-Oligocene transition The Eocene-Oligocene transition (~ 34 Ma) reflects a major step in the Cenozoic global climate change from a warm *greenhouse* climate to a cold *icehouse* climate. Besides large ice build up on Antarctica a major cooling is associated with this transition. At present, the most likely mechanism involved in the Eocene-Oligocene climate transition (EOT) is thought to be decreasing atmospheric CO_2 concentration to below a threshold that allows rapid

ice sheet growth on Antarctica.

In [26,27] it was shown that coupled NCAR Community Climate System Model (CCSM) simulations produced a good fit to paleoclimate proxy data across the EOT although the CO_2 changes required to accomplish this were arguably too large. In [28] late Eocene and early Oligocene pCO_2 was reconstructed. Here we use this information to estimate the palaeo climate sensitivity (or Earth system sensitivity) in two ways.

In the first case we utilize the model derived temperature change across the EOT and the newly reconstructed CO_2 change across this interval to estimate the Earth system sensitivity across the EOT. We use a late Eocene CO_2 value of 900 ppm and a range of early Oligocene values (500 ppmv, 600 ppmv and 700 ppmv) to define the possible radiative forcing across the transition ($\Delta R_{[CC]} = 5.38 \ln$(late Eocene/early Oligocene). Because of the good model fit to sparse proxy data we can utilize the modelled temperature change across the EOT. We use two modeled global mean values that span the time range of the late Eocene ($T_1^E = 25.7°C$, $T_2^E = 23.0°C$) and one value ($T_2^O = 20.9°C$) for the early Oligocene to calculate the global mean temperature change ΔT and a measure of uncertainty. Employing this range of values our estimate of the Earth System sensitivity $S^p = \Delta T / \Delta R_{CC}$ across the EOT is mean$(S^p) = 1.72$ K (W m^{-2})$^{-1}$, min$(S^p) = 0.65$ K (W m^{-2})$^{-1}$ and max$(S^p) = 3.51$ K (W m^{-2})$^{-1}$.

Using the same data but using the late Eocene and modern conditions as endpoints we can estimate the Earth System sensitivity between present day and Eocene values. Using the same two late Eocene temperature estimates and using a range of pCO_2 (1000 ppmv, 900 ppmv, 800 ppmv) and comparing with present day conditions (where present day conditions are defined by the configuration of an CAM3 AMIP simulation, with observed SSTs and $pCO_2 = 384$ ppmv) we can calculate a late Eocene to modern Earth System sensitivity. This estimate of S^p is mean$(S^p) = 1.818$ K (W m^{-2})$^{-1}$, min$(S^p) = 1.379$ K (W m^{-2})$^{-1}$ and max$(S^p) = 2.347$ K (W m^{-2})$^{-1}$.

To determine the Charney sensitivity S^a from these data, we would need to correct for land ice and vegetation changes as well as orography and continental geometry differences (i.e. calculate $S_{[CC,LI,VEG,OR]}$. The latter will be small for the Eocene to Oligocene case, but very large for the Eocene to present-day case.

B.4 The Palaeocene-Eocene Thermal Maximum The Palaeocene-Eocene Thermal Maximum (PETM, ∼56 Ma BP) is the most pronounced of at least four transient global warming events associated with massive and rapid carbon input into the global exogenic carbon pool [29,30]. These *hyperthermals* bear analogies to modern trends regarding carbon injection and global warming. However the lack of information regarding background conditions, rates of change and cause and effect, complicate direct comparison. The source of carbon is under debate and still viable hypotheses include biogenic[31,32] or thermogenic[33] CH_4 , and organic carbon[34]. Notably, if CH_4 was the primary source, the increase in radiative forcing must have been dominantly through CO_2 because of the short residence time of CH_4 in the ocean-atmosphere system[35,36]. All other changes in the concentrations of other greenhouse gases would have been a feedback to carbon injection or warming and is therefore included in the estimate of S.

The PETM is certainly the best-documented hyperthermal. At least at 12 sites in the ocean and on land, spanning tropical to polar locations, the increase in surface temperature has been quantified with high-quality data[37–47]. Based on these data, the estimated average surface warming is 5-6 K. On average, deep ocean temperatures increased by the same magnitude[38,48–50]. The increase in Arctic and deep ocean temperatures was of the same magnitude as in the tropics. Although warming in the Southern Ocean was perhaps somewhat larger[42,51], this indicates that polar amplification of this warming was absent or minor[41,50]. This is generally explained by the lack of a significant snow or ice albedo effect, since the latest Palaeocene likely was largely free of snow and ice[41]. We can therefore quantify ΔT = $5 - 6$ K. The uncertainty of this value is as in the Pliocene very difficult to determine due to the even more sparse and uneven data coverage for the PETM. In the calculations of S for the PETM in Table 1 (main text), we have therefore taken the precaution to allow an extra ± 1 K uncertainty in ΔT, although that may even be an underestimate.

More discussion remains on the absolute values and magnitude of increase in greenhouse gas concentrations. Two approaches have so far been employed to quantify carbon input during the PETM.

1. All hyperthermals are associated with a negative excursion in the stable carbon isotopic composition δ^{13}C of the exogenic carbon pool, reflecting the injection of ^{13}C-depleted carbon into the system[32]. The magnitude of this carbon isotope excursion (CIE) should relate to

the mass and δ^{13}C of the exogenic carbon cycle prior to the carbon injection, and the changes in carbon fluxes during the event, including the size and δ^{13}C of the net carbon influx[52]. By assuming various carbon reservoirs as a source and their intrinsic δ^{13}C value, the mass of carbon required to generate the CIE in the exogenic carbon pool can be calculated[52]. At least two problems rise with this approach: 1) different substrates and locations record a different magnitude of the CIE so discussion remains on the magnitude of the CIE in the global exogenic carbon pool[29,53], and 2) the CIE may have been a result of carbon release from multiple reservoirs[54,55]. The resulting uncertainty in estimating ΔR is very large.

2. The injected carbon will mostly reside in the ocean where it is buffered by the dissolution of sedimentary calcium carbonate. Indeed, significant decreases in calcite preservation has led to clay-rich layers in the major ocean basins[56,57]. The magnitude of dissolution in the global ocean should be equivalent to the late Paleocene state of the carbonate system and the total mass of injected carbon[31]. Two papers have so far attempted to quantify the carbon input based on this principle using carbon cycle modelling. The models include very different assumptions regarding late Paleocene ocean carbonate chemistry (notably the depth of the calcite compensation depth). Therefore, the amount of carbon required to generate the clay layers in the models differs significantly between these studies[55,58]. We use the upper and lower limits from these model studies to cover the uncertainty of ΔR. The most dramatic scenario implies only a factor 1.70 increase in CO_2 (less than a doubling), while the least dramatic suggests slightly less than a 3-fold increase. This represents the uncertainty in S in Table 1 (main text).

Several authors have suggested, based on high-resolution temperature proxy records, that part of the PETM warming (up to 3 K) occurred several ka prior to the onset of the CIE[51,54]. Potentially, this warming was regional, reflecting circulation change[59]. But if global, this warming can thus not have been caused by the same carbon that forced the CIE. If it was forced by carbon, this carbon must have had an isotopic composition close to that of the late Paleocene exogenic carbon pool[54]. Alternatively, the warming was not forced by carbon. Even though a mechanism is currently lacking for this hypothesis, the calculated value for S would in this case represent an overestimate.

C. Comparison of different estimates for the Charney climate sensitivity

Several estimates of the Charney climate sensitivity S^a have been produced recently with sometimes slightly different assumptions. Here we rephrase three estimates such that we can produce a proper intercomparison. In this section we explain how we can compare the work presented in the previous section which is based on a detailed assessment of paleodata over the last 800 kyr[4] and the studies by Hansen and Sato[5] also on the last 800 kyr and the work by van de Wal et al.[60] over the last 20 Ma. The aim is to come to calcuations of temperature change as a function of atmospheric CO_2 covering the range from LGM to $2\times CO_2$.

Consider that the climate sensitivity is affected by the following slow feedbacks: land ice (LI), vegetation (VG), aerosols (AE). Using the specific climate sensitivities

$$S_{[GHG]} = \frac{\Delta T}{\Delta R_{[GHG]}}, \tag{43a}$$

$$S_{[GHG,LI]} = \frac{\Delta T}{\Delta R_{[GHG]} + \Delta R_{[LI]}} \tag{43b}$$

we find

$$\frac{S_{[GHG]}}{S_{[GHG,LI]}} = 1 + \frac{\lambda_{LI}}{\lambda^f}, \tag{44}$$

where again $\lambda_{[X]} = \Delta R_{[X]}/\Delta T$ and $\lambda^f = \Delta R_{[GHG]}/\Delta T$ (as they are all considered as 'forcings'). In the same way, we find

$$\lambda_{LI} = \left(\frac{S_{[GHG]}}{S_{[GHG,LI]}} - 1\right)\lambda^f, \tag{45a}$$

$$\lambda_{VG} = \left(\frac{S_{[GHG]}}{S_{[GHG,LI,VG]}} - 1\right)\lambda^f - \lambda_{LI}, \tag{45b}$$

$$\lambda_{AE} = \left(\frac{S_{[GHG]}}{S_{[GHG,LI,AE]}} - 1\right)\lambda^f - \lambda_{LI}. \tag{45c}$$

We can use these relations to estimate temperature change ΔT due to a change in carbon dioxide. If we define the parameter F through

$$\Delta R_{[GHG,LI,AE,VG]} = \Delta R_{[GHG]} + \Delta R_{[LI]} + \Delta R_{[AE]} + \Delta R_{[VG]} = \frac{\Delta R_{[GHG]}}{1-F}, \tag{46}$$

then F combines the total effect of all the slow processes contained in land ice (LI), aerosol (AE), and vegetation (VG).

Using the following identity (showing again that climate sensitivity linearly relates temperature response to forcing)

$$\Delta T = S_{[GHG]}\Delta R_{[GHG]} = S_{[GHG,LI,AE,VG]}\Delta R_{[GHG,LI,AE,VG]}, \tag{47}$$

we find

$$\lambda^s = \lambda_{LI} + \lambda_{VG} + \lambda_{AE} = \left(\frac{S_{[GHG]}}{S_{[GHG,LI,AE,VG]}} - 1\right)\lambda^f. \tag{48}$$

Combining (46) and (48) yields

$$\lambda^s = \left(\frac{\Delta R_{[GHG,LI,AE,VG]}}{\Delta R_{[GHG]}} - 1\right)\lambda^f, \tag{49}$$

and hence we can define F in terms of the feedback parameters

$$F = \frac{\lambda^s}{\lambda^f + \lambda^s}. \tag{50}$$

This allows us to write a general expression for the temperature change due a change in radiative forcing caused by a change in CO_2

$$\Delta T = \gamma\frac{S_{[GHG,LI,AE,VG]}\Delta R_{[\mathrm{CO_2}]}}{1-F}, \tag{51}$$

with γ being the ratio between total greenhouse gas (GHG) forcing (CO_2, CH_4, N_2O) and CO_2 only

$$\gamma = \frac{\Delta R_{[GHG]}}{\Delta R_{[\mathrm{CO_2}]}}, \tag{52}$$

and with the CO_2 forcing given by[61]

$$\Delta R_{[\mathrm{CO_2}]} = \beta \ln\frac{\mathrm{CO_2}}{\mathrm{CO_{2,ref}}}, \tag{53}$$

where $\beta = 5.35$ W m^{-2}. The latter implies that we get $\Delta R = 3.7$ W m^{-2} for a doubled CO_2 forcing with respect to pre-industrial values. So we can formulate an expression for the global equilibrium temperature change as a function of the CO_2 concentration as

$$\Delta T = \gamma\beta\frac{S_{[GHG,LI,AE,VG]}}{1-F}\ln\frac{\mathrm{CO_2}}{\mathrm{CO_{2,ref}}}. \tag{54}$$

As discussed in part B.1, the mean climate sensitivity parameter S for the whole 800 kyr $S^{800\mathrm{k}}$ and the LGM S^{LGM} differ (Supplementary Table 1). This might be partially caused by a state-dependence of S, but might also be influenced by the fact that climate is not in (quasi-) equilibrium throughout the last 800 kyr. To check if there might be any transient effects in the data, we

restricted in a revised analysis the data sets to points, in which the temporal gradient in temperature $|\partial T/\partial t| < 0.5$ K per kyr. This gradient threshold implies that all data points in the LGM ($19-23$ ka BP) are then considered to be in equilibrium. In a second test an even stricter threshold of $|\partial T/\partial t| < 0.1$ K per kyr is considered. Both tests showed, that there is hardly any transient effect in the data; results are nearly identical to those obtained for the selected 800 kyr (lower half of Supplementary Table 1). We can therefore conclude that the different values of S for LGM or the whole 800 kyr are non-stationary. However, no clear relationship between S and the climate state emerges ($r^2 < 0.3$ of linear relationship between S and either ΔT or ΔR). Also the long-term evolution in S depicted in its 100-kyr running mean does not show any clear pattern (Supplementary Fig. S4C, Fig. S5C, Fig. 6C). However, the difference of calculated values of S for the well-defined stable climate of the LGM from the mean over the last 800 kyr falls well within the uncertainties given, in particular when the slow feedbacks are incorporated as forcing. Thus, we will use in the following results obtained for the 800 kyr data set, but should keep in mind that corrections for state-dependence might be applicable once they are available. So far, we know from previous studies[7,8] that the climate sensitivity parameters depend on climate state, but by how much is model-dependent[6,7,62].

Application of the values obtained for the last 800 kyr, as summarised in Supplementary Table 1 (using Eqs 14, 45, 48 and 50) yields the following values for the feedback parameters ($\pm$ 1 σ):

$$\lambda^f = 0.47 \pm 0.10 \text{ W m}^{-2} \text{ K}^{-1}, \tag{55a}$$

$$\lambda_{LI} = 0.67 \pm 0.18 \text{ W m}^{-2} \text{ K}^{-1}, \tag{55b}$$

$$\lambda_{VG} = 0.22 \pm 0.19 \text{ W m}^{-2} \text{ K}^{-1}, \tag{55c}$$

$$\lambda_{AE} = 0.23 \pm 0.13 \text{ W m}^{-2} \text{ K}^{-1}, \tag{55d}$$

$$\lambda^s = 1.12 \pm 0.29 \text{ W m}^{-2} \text{ K}^{-1} \tag{55e}$$

$$\text{and hence } F = 0.71 \pm 0.23. \tag{55f}$$

To determine how the equilibrium temperature change is related to CO_2 changes we might either consider all (slow and fast) feedbacks ($F = 0.71 \pm 0.23$) resembling long-term changes on orbital time scales, or consider only the fast and neglect the slow feedbacks ($F = 0.0$) mimicking the

Charney sensitivity for the next century.

$$\Delta T_{\text{This study}} = \gamma\beta \frac{S^{800\text{k}}_{[GHG,LI,AE,VG]}}{1-F} \ln \frac{\text{CO}_2}{\text{CO}_{2,\text{ref}}} \quad \text{(all feedbacks)}, \tag{56a}$$

$$\Delta T_{\text{This study}} = \gamma\beta S^{800\text{k}}_{[GHG,LI,AE,VG]} \ln \frac{\text{CO}_2}{\text{CO}_{2,\text{ref}}} \quad \text{(fast feedbacks)}. \tag{56b}$$

The second attempt to quantify the climate sensitivity parameter is based on van de Wal et al.[60] who compiled CO_2 proxies and temperature data over the last 20 million years to evaluate the CO_2 concentration over this period. Temperature data are as in the previous section based on an inverse modelling exercise where the marine benthic record is assimilated (van de Wal et al., 2011[60], abbreviated here to RW11). RW11 does not allow as much detail as can be obtained over the last 800 ka, but the advantage is that it covers also somewhat warmer climates than just the last 800 ka. RW11 present the following expression for the temperature change as a function of CO_2:

$$\Delta T_{RW11} = \frac{C}{a} \ln \frac{\text{CO}_2}{\text{CO}_{2,\text{ref}}} \quad \text{(all feedbacks)}, \tag{57a}$$

$$\Delta T_{RW11} = \frac{C}{a} \ln \frac{\text{CO}_2}{\text{CO}_{2,\text{ref}}} (1-F) \quad \text{(fast feedbacks)}, \tag{57b}$$

with $C = 39 \pm 4$ K and where a is the polar amplification factor of 2.7 ± 0.25 which relates the change in Northern Hemisphere temperatures to global temperature changes, including slow feedbacks. In order to reconstruct the temperature without slow feedbacks, the equation needs to be multiplied by $(1-F)$ where $F = 0.71$ is the slow feedback factor[60]. The calculation of F is based on the same data set as above[4], so the same uncertainties in F are assumed ($\sigma_F = 0.23$).

Finally we consider the study by Hansen and Sato[5] who define a fast feedback sensitivity of $S_{ff} = 0.75 \pm 0.125$ K (W m^{-2})$^{-1}$ and a total sensitivity (fast and surface) of $S_{ff+sur} = 1.5 \pm 0.1875$ K (W m^{-2})$^{-1}$. From these two values we can derive with the definition of F (Eq. 46) both the fast $\lambda^f = 1.33 \pm 0.22$ W m^{-2} K^{-1} and slow $\lambda^s = 1.33 \pm 0.17$ W m^{-2} K^{-1} feedback parameter and with Eq. 50 that $F = 0.50 \pm 0.08$. To take the effect of non-CO_2 greenhouse gases (CH_4, N_2O) into account we use again the factor $\gamma = 1.33$ as also done above.

$$\Delta T_{JH12} = \gamma\beta \frac{S_{ff}}{1-F} \ln \frac{\text{CO}_2}{\text{CO}_{2,\text{ref}}} \quad \text{(all feedbacks)}, \tag{58a}$$

$$\Delta T_{JH12} = \gamma\beta S_{ff} \ln \frac{\text{CO}_2}{\text{CO}_{2,\text{ref}}} \quad \text{(fast feedbacks)}. \tag{58b}$$

Again F is introduced to distinguish between cases including slow feedbacks ($F = 0.5$) and cases that neglect slow feedbacks ($F = 0$).

Following the analysis in part C of the supplementary information that culminates in Eqs. (56-58), we present in Fig. 4 (main text) an overview of the three different studies.

Supplementary References

1. Hansen, J. *et al.* Climate sensitivity: Analysis of feedback mechanisms. In Hansen, J. & Takahashi, T. (eds.) *Climate Processes and Climate Sensitivity*, vol. 29 of *Geophysical Monographs*, 130–163 (American Geophysical Union, Washington, USA, 1984).

2. Roe, G. Feedbacks, timescales, and seeing red. *Annual Review in Earth and Planetary Sciences* **37**, 93–115 (2009). doi: 10.1146/annurev.earth.061008.134734.

3. Charney, J. G. *et al.* *Carbon Dioxide and Climate: A Scientific Assessment* (National Academy of Science, Washington, D.C., 1979).

4. Köhler, P. *et al.* What caused Earth's temperature variations during the last 800,000 years? Data-based evidences on radiative forcing and constraints on climate sensitivity. *Quaternary Science Reviews* **29**, 129–145 (2010). doi: 10.1016/j.quascirev.2009.09.026.

5. Hansen, J. E. & Sato, M. Paleoclimate Implications for Human-Made Climate Change. In Berger, A., Mesinger, F. & Šijački, D. (eds.) *Climate Change: Inferences from Paleoclimate and Regional Aspects*, 21–48 (Springer, 2012). doi: 10.1007/978-3-7091-0973-1_2.

6. Crucifix, M. Does the Last Glacial Maximum constrain climate sensitivity? *Geophysical Research Letters* **33**, L18701, doi: 10.1029/2006GL027137 (2006).

7. Hargreaves, J. C., Abe-Ouchi, A. & Annan, J. D. Linking glacial and future climates through an ensemble of GCM simulations. *Climate of the Past* **3**, 77–87 (2007).

8. Yoshimori, M., Hargreaves, J. C., Annan, J. D., Yokohata, T. & Abe-Ouchi, A. Dependency of Feedbacks on Forcing and Climate State in Physics Parameter Ensembles. *Journal of Climate* **24**, 6440–6455 (2011). doi: 10.1175/2011JCLI3954.1.

9. Bintanja, R., van de Wal, R. & Oerlemans, J. Modelled atmospheric temperatures and global sea levels over the past million years. *Nature* **437**, 125–128, doi: 10.1038/nature03975 (2005).

10. Lisiecki, L. E. & Raymo, M. E. A Pliocene-Pleistocene stack of 57 globally distributed benthic δ^{18}O records. *Paleoceanography* **20**, PA1003, doi: 10.1029/2004PA001071 (2005).

11. Schneider von Deimling, T., Ganopolski, A., Held, H. & Rahmstorf, S. How cold was the Last Glacial Maximum? *Geophysical Research Letters* **33**, L14709, doi: 10.1029/2006GL026484 (2006).

12. Singarayer, J. S. & Valdes, P. J. High-latitude climate sensitivity to ice-sheet forcing over the last 120kyr. *Quaternary Science Reviews* **29**, 43 – 55 (2010). doi: 10.1016/j.quascirev.2009.10.011.

13. Lunt, D. J. *et al.* Earth system sensitivity inferred from Pliocene modelling and data. *Nature Geoscience* **3**, 60–64 (2010). doi: 10.1038/ngeo706.

14. Seki, O. *et al.* Alkenone and boron-based Pliocene pCO(2) records. *Earth and Planetary Science Letters* **292**, 201–211 (2010). doi: 10.1016/j.epsl.2010.01.037.

15. Pagani, M., Liu, Z., LaRiviere, J. & Ravelo, A. C. High Earth-system climate sensitivity determined from Pliocene carbon dioxide concentrations. *Nature Geoscience* **3**, 27–30 (2010).

16. Bartoli, G., Hoenisch, B. & Zeebe, R. E. Atmospheric CO(2) decline during the Pliocene intensification of Northern Hemisphere glaciations. *Paleoceanography* **26** (2011). doi: 10.1029/2010PA002055.

17. Dowsett, H. J. & Robinson, M. M. Mid-pliocene planktic foraminifer assemblage of the north Atlantic ocean. *Micropaleontology* **53**, 105–126 (2007).

18. Dowsett, H. J., Robinson, M. M., Stoll, D. K. & Foley, K. M. Mid-Piacenzian mean annual sea surface temperature analysis for data-model comparisons. *Stratigraphy* **7**, 189–198 (2010).

19. Dowsett, H. J. *et al.* Sea surface temperatures of the mid-Piacenzian Warm Period: A comparison of PRISM3 and HadCM3. *Palaeogeography, Palaeoclimatology, Palaeoecology* **309**, 83 – 91 (2011). doi: 10.1016/j.palaeo.2011.03.016.

20. Thompson, R. & Fleming, R. Middle Pliocene vegetation: Reconstructions, paleoclimatic inferences, and boundary conditions for climate modeling. *Marine Micropaleontology* **27**, 27–49 (1996). doi: 10.1016/0377-8398(95)00051-8.

21. Dowsett, H. *et al.* Joint investigations of the Middle Pliocene climate .1. PRISM paleoenvironmental reconstructions. *Global and Planetary Change* **9**, 169–195 (1994). doi: 10.1016/0921-8181(94)90015-9.

22. Lunt, D. J. *et al.* On the causes of mid-Pliocene warmth and polar amplification. *Earth and Planetary Science Letters* **321–322**, 128 – 138 (2012). doi: 10.1016/j.epsl.2011.12.042.

23. Hansen, J. *et al.* Efficacy of climate forcings. *Journal of Geophysical Research* **110**, D18104 (2005). doi: 10.1029/2005JD005776.

24. Markwick, P. J. The palaeogeographic and palaeoclimatic significance of climate proxies for data-model comparisons. In Haywood, A., Gregory, F. J. Schmidt, D. N. (eds.) *Deep time perspectives on Climate Change: Marrying the Signal from Computer Models and Biological Proxies*, 323–347 (The Micropalaeontological Society, Special Publications. The Geological Society, London, 2007).

25. Haywood, A. M. *et al.* Pliocene Model Intercomparison Project (PlioMIP): experimental design and boundary conditions (Experiment 2). *Geoscientific Model Development* **4**, 571–577 (2011). doi: 10.5194/gmd-4-571-2011.

26. Liu, Z. *et al.* Global Cooling During the Eocene-Oligocene Climate Transition. *Science* **323**, 1187–1190 (2009). doi: 10.1126/science.1166368.

27. Eldrett, J. S., Greenwood, D. R., Harding, I. C. & Huber, M. Increased seasonality through the Eocene to Oligocene transition in northern high latitudes. *Nature* **459**, 969–974 (2009). doi: 10.1038/nature08069.

28. Pagani, M. *et al.* The Role of Carbon Dioxide During the Onset of Antarctic Glaciation. *Science* **334**, 1261–1264 (2011). doi: 10.1126/science.1203909.

29. McInerney, F. A. & Wing, S. L. The Paleocene-Eocene Thermal Maximum: A Perturbation of Carbon Cycle, Climate, and Biosphere with Implications for the Future. *Annual Review of Earth and Planetary Sciences* **39**, 489–516 (2011). doi: 10.1146/annurev-earth-040610-133431.

30. Sluijs, A., Bowen, G. J., Brinkhuis, H., Lourens, L. J. & Thomas, E. The Palaeocene-Eocene thermal maximum super greenhouse: biotic and geochemical signatures, age models and mechanisms of global change. In Williams, M., Haywood, A., Gregory, J. & Schmidt, D. (eds.) *Deep time perspectives on Climate Change: Marrying the Signal from Computer Models and Biological Proxies*, 323–347 (The Micropalaeontological Society, Special Publications. The Geological Society, London, 2007).

31. Dickens, G. R., Castillo, M. M. & Walker, J. C. G. A blast of gas in the latest Paleocene: Simulating first-order effects of massive dissociation of oceanic methane hydrate. *Geology* **25**, 259–262 (1997). doi: 10.1130/0091-7613(1997)025<0259:ABOGIT>2.3.CO;2.

32. Dickens, G. R., O'Neil, J. R., Rea, D. K. & Owen, R. M. Dissociation of Oceanic Methane Hydrate as a Cause of the Carbon Isotope Excursion at the End of the Paleocene. *Paleoceanography* **10**, 965–971 (1995). doi: 10.1029/95PA02087.

33. Svensen, H. *et al.* Release of methane from a volcanic basin as a mechanism for initial Eocene global warming. *Nature* **429**, 542–545 (2004). doi: 10.1038/nature02566.

34. Kurtz, A. C., Kump, L. R., Arthur, M. A., Zachos, J. C. & Paytan, A. Early Cenozoic decoupling of the global carbon and sulfur cycles. *Paleoceanography* **18**, 1090 (2003). doi: 10.1029/2003PA000908.

35. Dale, A., Cappellen, P. V., Aguilera, D. & Regnier, P. Methane efflux from marine sediments in passive and active margins: Estimations from bioenergetic reaction-transport simulations. *Earth and Planetary Science Letters* **265**, 329 – 344 (2008). doi: 10.1016/j.epsl.2007.09.026.

36. Schmidt, G. A. & Shindell, D. T. Atmospheric composition, radiative forcing, and climate change as a consequence of a massive methane release from gas hydrates. *Paleoceanography* **18**, 1004 (2003). doi: 10.1029/2002PA000757.

37. John, C. M. *et al.* North American continental margin records of the Paleocene-Eocene thermal maximum: Implications for global carbon and hydrological cycling. *Paleoceanography* **23**, PA2217 (2008). doi: 10.1029/2007PA001465.

38. Kennett, J. P. & Stott, L. D. Abrupt deep-sea warming, palaeoceanogrphcial changes and benthic extinctions at the end of the Paleocene. *Nature* **353**, 225–229 (1991). doi: 10.1038/353225a0.

39. Kelly, D., Bralower, T. J. & Zachos, J. C. Evolutionary consequences of the latest Paleocene thermal maximum for tropical planktonic foraminifera. *Palaeogeography, Palaeoclimatology, Palaeoecology* **141**, 139 – 161 (1998). doi: 10.1016/S0031-0182(98)00017-0.

40. Kozdon, R., Kelly, D. C., Kita, N. T., Fournelle, J. H. & Valley, J. W. Planktonic foraminiferal oxygen isotope analysis by ion microprobe technique suggests warm tropical sea surface temperatures during the Early Paleogene. *Paleoceanography* **26**, PA3206 (2011). doi: 10.1029/2010PA002056.

41. Sluijs, A. *et al.* Subtropical Arctic Ocean temperatures during the Palaeocene/Eocene thermal maximum. *Nature* **441**, 610–613 (2006). doi: 10.1038/nature04668.

42. Sluijs, A. *et al.* Southern ocean warming, sea level and hydrological change during the Paleocene-Eocene thermal maximum. *Climate of the Past* **7**, 47–61 (2011). doi: 10.5194/cp-7-47-2011.

43. Tripati, A. K. & Elderfield, H. Abrupt hydrographic changes in the equatorial Pacific and subtropical Atlantic from foraminiferal Mg/Ca indicate greenhouse origin for the thermal maximum at the Paleocene-Eocene Boundary. *Geochemistry, Geophysics, Geosystems* **5**, Q02006 (2004). doi: 10.1029/2003GC000631.

44. Weijers, J. W., Schouten, S., Sluijs, A., Brinkhuis, H. & Damsté, J. S. S. Warm arctic continents during the Palaeocene-Eocene thermal maximum. *Earth and Planetary Science Letters* **261**, 230 – 238 (2007). doi: 10.1016/j.epsl.2007.06.033.

45. Wing, S. L. *et al.* Transient Floral Change and Rapid Global Warming at the Paleocene-Eocene Boundary. *Science* **310**, 993–996 (2005). doi: 10.1126/science.1116913.

46. Zachos, J. *et al.* Extreme warming of mid-latitude coastal ocean during the Paleocene-Eocene Thermal Maximum: Inferences from TEX_{86} and isotope data. *Geology* **34**, 737–740 (2006). doi: 10.1130/G22522.1.

47. Zachos, J. C. *et al.* A Transient Rise in Tropical Sea Surface Temperature During the Paleocene-Eocene Thermal Maximum. *Science* **302**, 1551–1554 (2003). doi: 10.1126/science.1090110.

48. Thomas, E. & Shackleton, N. J. The Paleocene-Eocene benthic foraminiferal extinction and stable isotope anomalies. *Geological Society, London, Special Publications* **101**, 401–441 (1996). doi: 10.1144/GSL.SP.1996.101.01.20.

49. McCarren, H., Thomas, E., Hasegawa, T., Rhl, U. & Zachos, J. C. Depth dependency of the Paleocene-Eocene carbon isotope excursion: Paired benthic and terrestrial biomarker records (Ocean Drilling Program Leg 208, Walvis Ridge). *Geochemistry, Geophysics, Geosystems* **9**, Q10008 (2008). doi: 10.1029/2008GC002116.

50. Tripati, A. & Elderfield, H. Deep-Sea Temperature and Circulation Changes at the Paleocene-Eocene Thermal Maximum. *Science* **308**, 1894–1898 (2005). doi: 10.1126/science.1109202.

51. Thomas, D. J., Zachos, J. C., Bralower, T. J., Thomas, E. & Bohaty, S. Warming the fuel for the fire: Evidence for the thermal dissociation of methane hydrate during the Paleocene-Eocene thermal maximum. *Geology* **30**, 1067–1070 (2002). doi: 10.1130/0091-7613(2002)030<1067:WTFFTF>2.0.CO;2.

52. Dickens, G. R. Carbon addition and removal during the Late Palaeocene Thermal Maximum: basic theory with a preliminary treatment of the isotope record at ODP Site 1051, Blake Nose. *Geological Society, London, Special Publications* **183**, 293–305 (2001). doi: 10.1144/GSL.SP.2001.183.01.14.

53. Dickens, G. R. Down the Rabbit Hole: toward appropriate discussion of methane release from gas hydrate systems during the Paleocene-Eocene thermal maximum and other past hyperthermal events. *Climate of the Past* **7**, 831–846 (2011). doi: 10.5194/cp-7-831-2011.

54. Sluijs, A. *et al.* Environmental precursors to rapid light carbon injection at the Palaeocene/Eocene boundary. *Nature* **450**, 1218–1221 (2007). doi: 10.1038/nature06400.

55. Panchuk, K., Ridgwell, A. & Kump, L. Sedimentary response to Paleocene-Eocene Thermal Maximum carbon release: A model-data comparison. *Geology* **36**, 315–318 (2008). doi: 10.1130/G24474A.1.

56. Colosimo, A. B., Bralower, T. J. & Zachos, J. C. Evidence for Lysocline Shoaling at the Paleocene/Eocene Thermal Maximum on Shatsky Rise, Northwest Pacific. In Bralower, T., Premoli Silva, I. & Malone, M. (eds.) *Proceedings of the Ocean Drilling Program, Scientific Results Vol 198 [Online]* (http://www-odp.tamu.edu/publications/198_SR/112.pdf, 2006). doi: 10.2973/odp.proc.sr.198.112.2006.

57. Zachos, J. C. *et al.* Rapid Acidification of the Ocean During the Paleocene-Eocene Thermal Maximum. *Science* **308**, 1611–1615 (2005). doi: 10.1126/science.1109004.

58. Zeebe, R. E., Zachos, J. C. & Dickens, G. R. Carbon dioxide forcing alone insufficient to explain Palaeocene-Eocene Thermal Maximum warming. *Nature Geoscience* **2**, 576–580 (2009). doi: 10.1038/ngeo578.

59. Lunt, D. J. *et al.* A model for orbital pacing of methane hydrate destabilization during the Palaeogene. *Nature Geoscience* **4**, 775–778 (2011). doi: 10.1038/ngeo1266.

60. van de Wal, R. S. W., de Boer, B., Lourens, L., Köhler, P. & Bintanja, R. Reconstruction of a continuous high-resolution CO_2 record over the past 20 million years. *Climate of the Past* **7**, 1459–1469 (2011). doi: 10.5194/cp-7-1459-2011.

61. Myhre, G., Highwood, E. J., Shine, K. P. & Stordal, F. New estimates of radiative forcing due to well mixed greenhouse gases. *Geophysical Research Letters* **25**, 2715–2718 (1998).

62. Colman, R. & McAvaney, B. Climate feedbacks under a very broad range of forcing. *Geophysical Research Letters* **36**, L01702, doi: 10.1029/2008GL036268 (2009).

Supplementary Table 1: Climate sensitivity parameter S based on different explicit considered forcings as compiled before[4]; S was not corrected for differences in climate state. In the specific climate sensitivities, $S_{[X,Y,...]}$ in the following rows the explicit forcings as defined in Table 2 are considered (main text). 800 ka selected: all data points of the last 800 ka which fulfil the threshold conditions (ΔT < -1.5 K and ΔR < -0.5 W m^{-2}). LGM: only data points in the time window $19 - 23$ ka BP. The lower half of the table contains further subsets of "800 ka selected", in which only data points during stable climate are considered, so further filtered by $|\delta T/\delta t| < 0.5$ K per kyr or $|\delta T/\delta t| < 0.1$ K per kyr. This selection should test if there are any transient effects (data not in equilibrium) in the data, but since the resulting S_X for all X are nearly identical to the subset of "800 ka selected" we conclude that there is only a small transient effect. K': number of data points. Given uncertainties σ is the larger of both σ_0 (averging uncertainty) and $\overline{\sigma_1}$ (mean of propagated uncertainty).

	$S \pm 1\sigma$ K/(W/m^2)	K' -	$S \pm 1\sigma$ K/(W/m^2)	K' -
	800 ka selected		LGM	
$S_{[CO_2]}$	3.08 $\pm$ 0.96 ($\pm$ 31%)	6615	2.63 $\pm$ 0.57 ($\pm$ 21%)	41
$S_{[CO_2,LI]}$	1.07 $\pm$ 0.40 ($\pm$ 37%)	6993	0.95 $\pm$ 0.22 ($\pm$ 23%)	41
$S_{[CO_2,LI,VG]}$	0.86 $\pm$ 0.27 ($\pm$ 31%)	7058	0.80 $\pm$ 0.19 ($\pm$ 23%)	41
$S_{[CO_2,LI,AE]}$	0.90 $\pm$ 0.42 ($\pm$ 46%)	7013	0.72 $\pm$ 0.18 ($\pm$ 25%)	41
$S_{[CO_2,LI,AE,VG]}$	0.75 $\pm$ 0.29 ($\pm$ 38%)	7064	0.63 $\pm$ 0.15 ($\pm$ 23%)	41
$S_{[GHG]}$	2.32 $\pm$ 0.76 ($\pm$ 32%)	6897	1.97 $\pm$ 0.41 ($\pm$ 20%)	41
$S_{[GHG,LI]}$	0.96 $\pm$ 0.36 ($\pm$ 37%)	7025	0.85 $\pm$ 0.19 ($\pm$ 22%)	41
$S_{[GHG,LI,VG]}$	0.78 $\pm$ 0.23 ($\pm$ 29%)	7064	0.73 $\pm$ 0.16 ($\pm$ 21%)	41
$S_{[GHG,LI,AE]}$	0.82 $\pm$ 0.36 ($\pm$ 43%)	7035	0.66 $\pm$ 0.16 ($\pm$ 24%)	41
$S_{[GHG,LI,AE,VG]}$	0.68 $\pm$ 0.24 ($\pm$ 35%)	7067	0.58 $\pm$ 0.14 ($\pm$ 24%)	41
	$\lvert\delta T/\delta t\rvert < 0.5$ K per kyr		$\lvert\delta T/\delta t\rvert < 0.1$ K per kyr	
$S_{[CO_2]}$	3.00 $\pm$ 0.98 ($\pm$ 32%)	5684	3.00 $\pm$ 1.01 ($\pm$ 33%)	1526
$S_{[CO_2,LI]}$	1.03 $\pm$ 0.39 ($\pm$ 37%)	6068	1.02 $\pm$ 0.33 ($\pm$ 32%)	1626
$S_{[CO_2,LI,VG]}$	0.84 $\pm$ 0.26 ($\pm$ 30%)	6109	0.83 $\pm$ 0.26 ($\pm$ 31%)	1637
$S_{[CO_2,LI,AE]}$	0.87 $\pm$ 0.40 ($\pm$ 45%)	6084	0.85 $\pm$ 0.34 ($\pm$ 40%)	1631
$S_{[CO_2,LI,AE,VG]}$	0.72 $\pm$ 0.26 ($\pm$ 36%)	6116	0.71 $\pm$ 0.25 ($\pm$ 35%)	1639
$S_{[GHG]}$	2.26 $\pm$ 0.78 ($\pm$ 34%)	5946	2.25 $\pm$ 0.83 ($\pm$ 36%)	1594
$S_{[GHG,LI]}$	0.92 $\pm$ 0.34 ($\pm$ 36%)	6085	0.91 $\pm$ 0.28 ($\pm$ 30%)	1629
$S_{[GHG,LI,VG]}$	0.76 $\pm$ 0.22 ($\pm$ 28%)	6116	0.76 $\pm$ 0.21 ($\pm$ 27%)	1639
$S_{[GHG,LI,AE]}$	0.79 $\pm$ 0.35 ($\pm$ 44%)	6103	0.77 $\pm$ 0.29 ($\pm$ 37%)	1633
$S_{[GHG,LI,AE,VG]}$	0.66 $\pm$ 0.22 ($\pm$ 33%)	6118	0.65 $\pm$ 0.21 ($\pm$ 32%)	1639

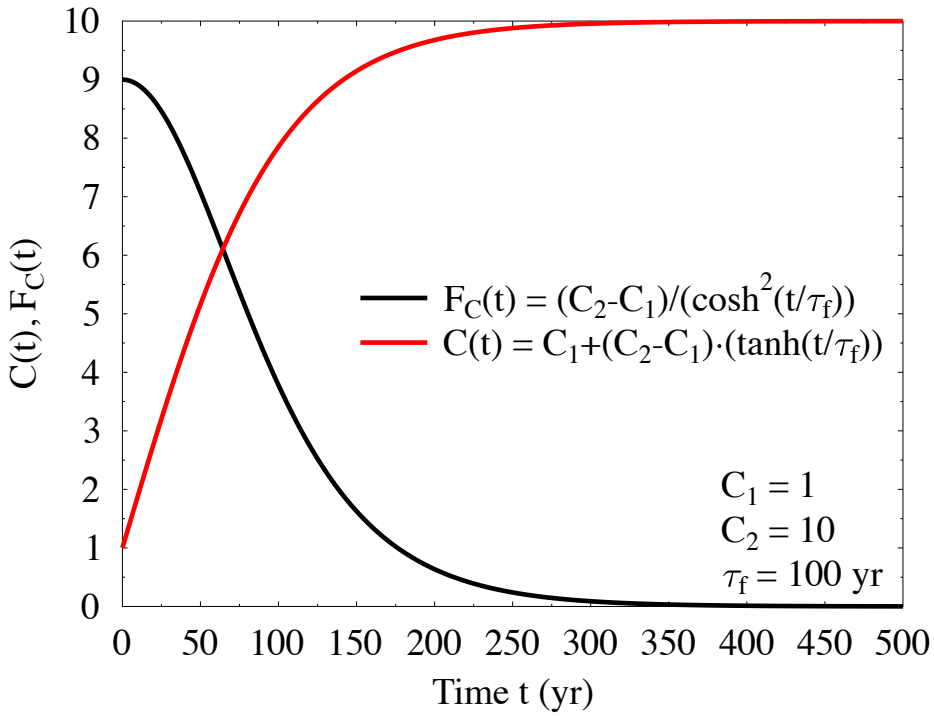

Figure 1 Illustrative examples of emission time series $F_C(t)$ and resulting atmospheric carbon $C(t)$ following Eqs. 8 and 9.

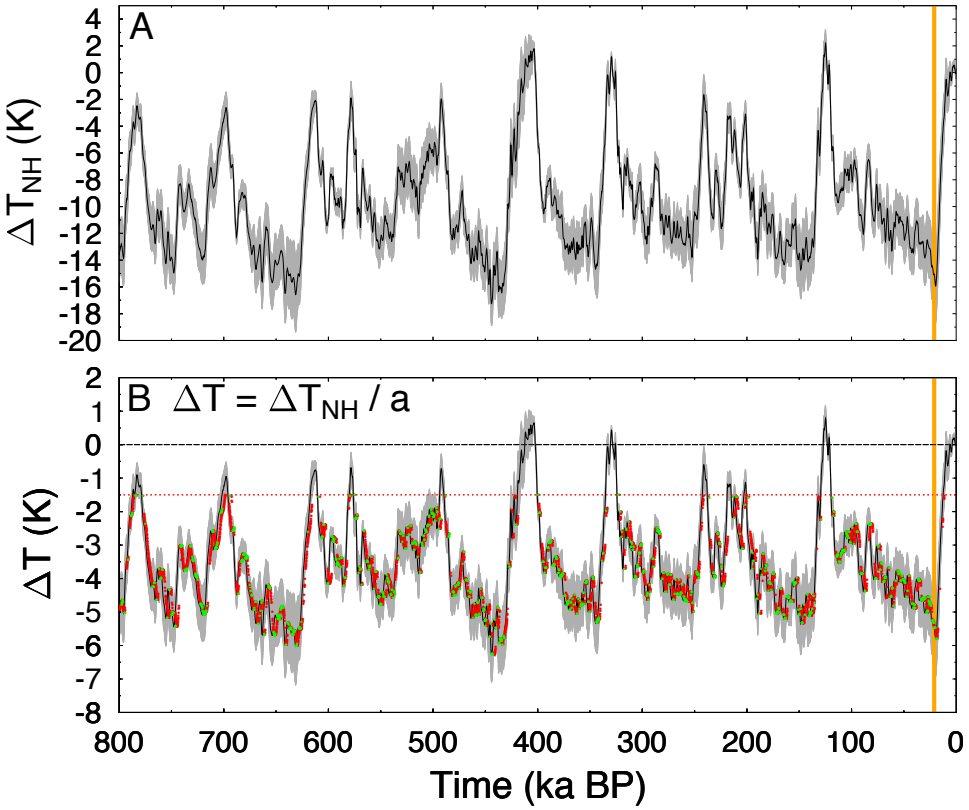

Figure 2 Temperature time series used for the calculation of S. A: The time series of temperature change on high northern hemispheric land ($40 - 80^\circ$ N) ΔT_{NH} deduced via an inverse modelling approach[9] from the benthic δ^{18}O stack[10]. B: Global temperature change ΔT derived from ΔT_{NH} using a polar amplification factor on northern high latitudes of $a = 2.75 \pm 0.25$. The red broken line indicates the threshold at $\Delta T = -1.5$ K below which ΔT needs to falls for the robust calculations on S. Coloured dots indicate data points which pass certain thresholds to reduce transient effect. The weak transient threshold (red, $|\partial T/\partial t| < 0.5$ K per kyr) implies that 80% of all data points, but all LGM data points are considered, the strong transient threshold (green, $|\partial T/\partial t| < 0.1$ K per kyr) implies only 21% of all data points, and only 37% of the LGM data points are considered. The grey bands give one σ uncertainties. Orange vertical bar denotes the LGM ($23 - 19$ ka BP).

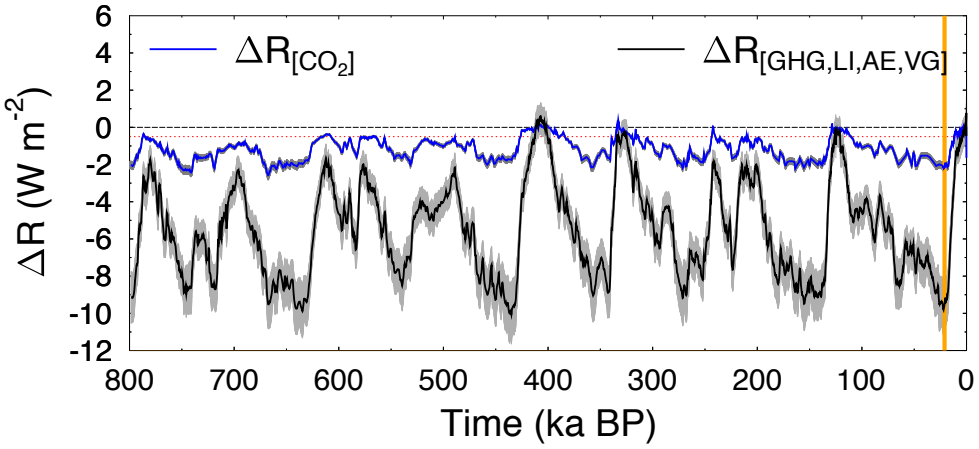

Figure 3 Radiative forcing ΔR time series used for the calculation of S. The two extreme examples are given here, where either only CO_2 is given as radiative forcing ($\Delta R_{[CO_2]}$), or where additionally all other radiative forcing is taken into consideration (CO_2, CH_4, N_2O, ice sheets, vegetation, aerosols) in $\Delta R_{[GHG,LI,AE,VG]}$. All other possible explicit forcings lie in in-between ΔR_{CO_2} and $\Delta R_{[GHG,LI,AE,VG]}$ and might be looked up in detail in the former study[4]. The grey band gives one $\sigma_{1,i}$ uncertainty. A calculated S is only considered robust when $\Delta R < -0.5$ W m^{-2} (indicated by the red broken lines). Orange vertical bar denotes the LGM ($23 - 19$ ka BP).

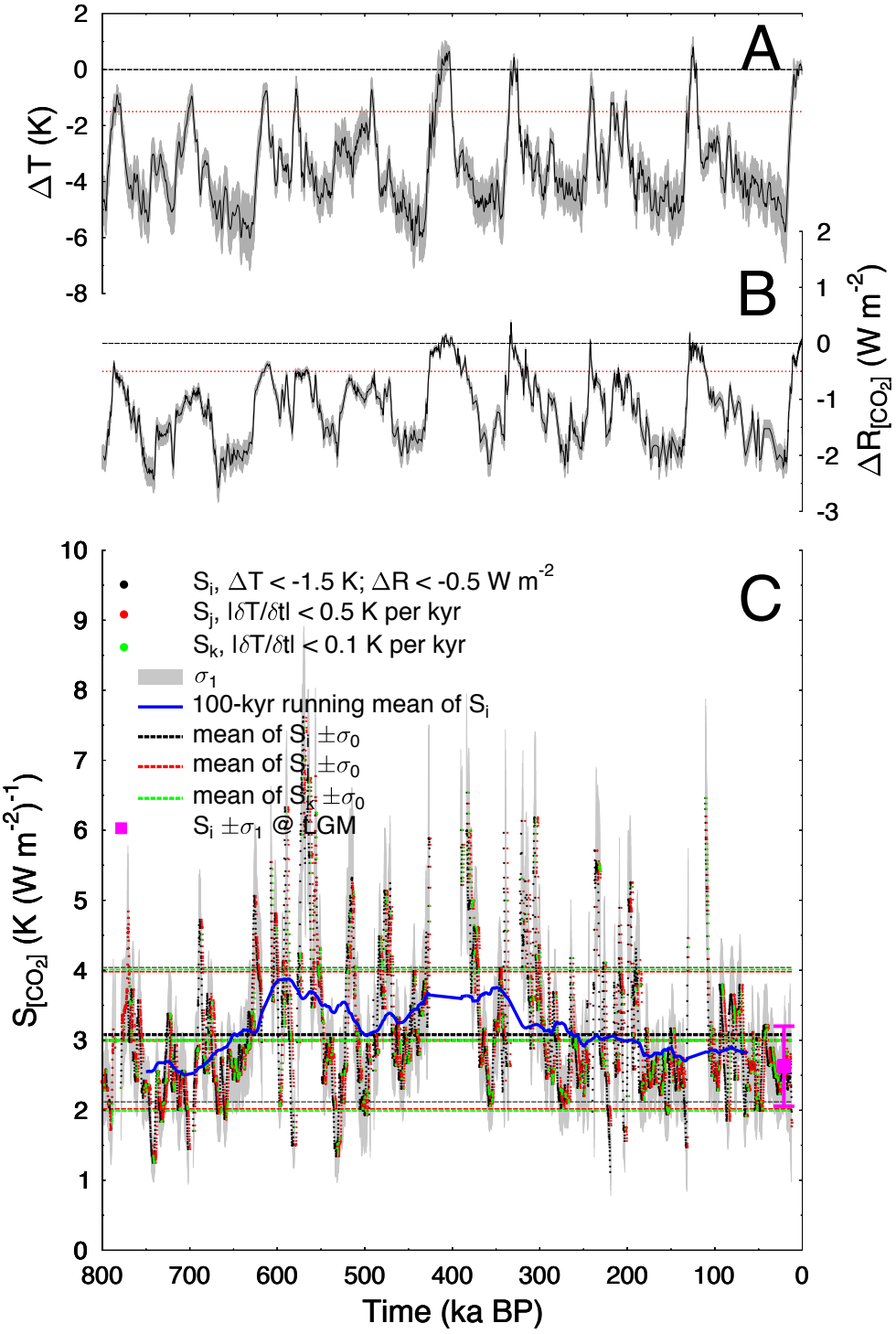

Figure 4 In-depth calculation of S for (C) $S_{[\mathrm{CO_2}]}$. (A) Considered global temperature, taken from Supplementary Figure 2. (B) Considered radiative forcing, taken from Supplementary Figure 3. Additional filters were implemented to avoid data with fast changes (transient effects). Filter was either weak (red, $|\partial T/\partial t| < 0.5$ K per kyr) or strong (green, $|\partial T/\partial t| < 0.1$ K per kyr). Mean of $S \pm \sigma_0$ for various selections and 100-kyr running mean are shown together with individual results for single points. Cyan markers denotes the $S \pm \sigma_0$ at the LGM ($23 - 19$ ka BP).

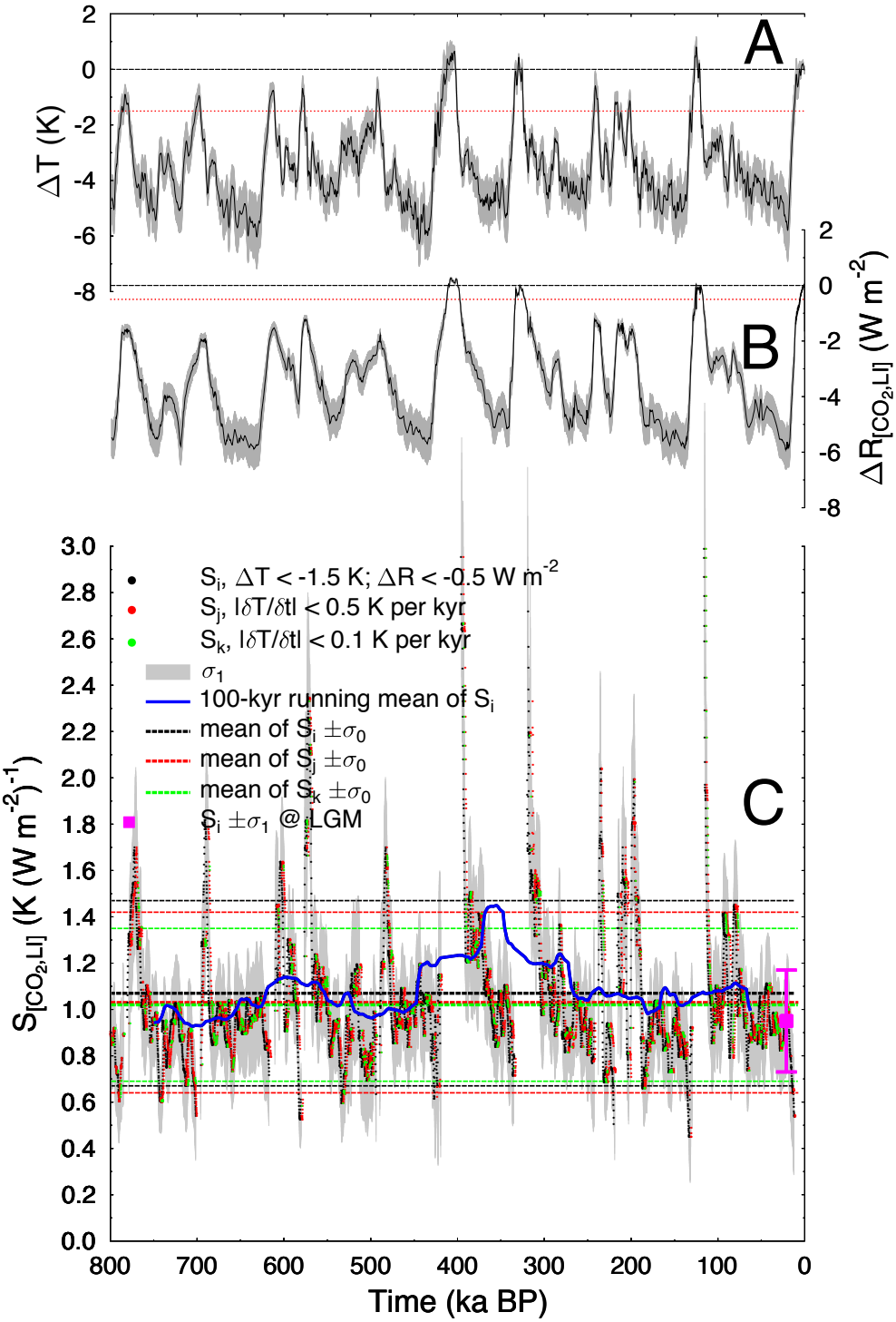

Figure 5 In-depth calculation of S for (C) $S_{[\mathrm{CO}_2,LI]}$. (A) Considered global temperature, taken from Supplementary Figure 2. (B) Considered radiative forcing. Additional filters were implemented to avoid data with fast changes (transient effects). Filter was either weak (red, $|\partial T/\partial t| < 0.5$ K per kyr) or strong (green, $|\partial T/\partial t| < 0.1$ K per kyr). Mean of $S \pm \sigma_0$ for various selections and 100-kyr running mean are shown together with individual results for single points. Magenta marker denotes the $S \pm \sigma_1$ at the LGM ($23 - 19$ ka BP).

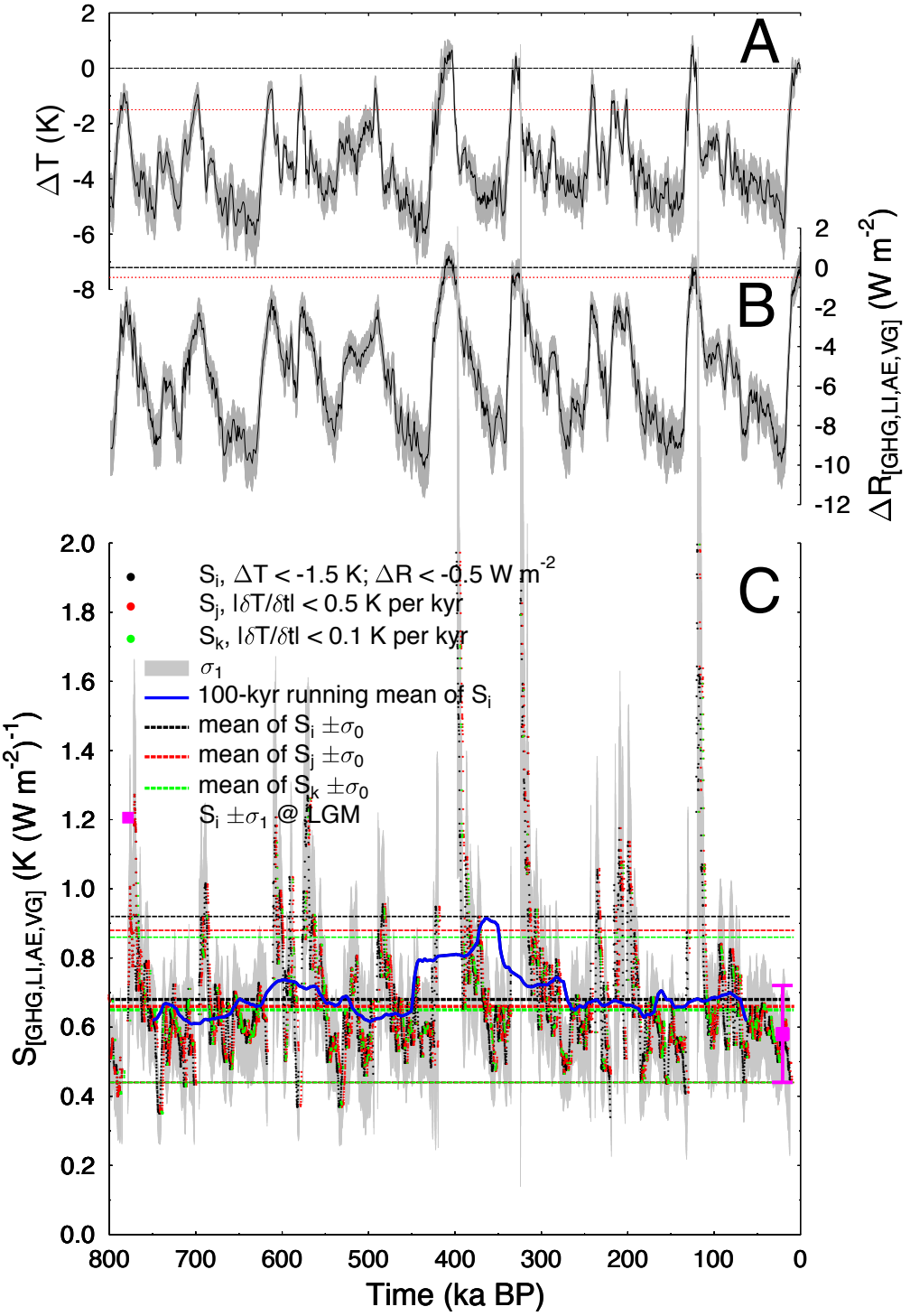

Figure 6 In-depth calculation of S for (C) $S_{[GHG,LI,AE,VG]}$. (A) Considered global temperature, taken from Supplementary Figure 2. (B) Considered radiative forcing, taken from Supplementary Figure 3. Additional filters were implemented to avoid data with fast changes (transient effects). Filter was either weak (red, $|\partial T/\partial t| < 0.5$ K per kyr) or strong (green, $|\partial T/\partial t| < 0.1$ K per kyr). Mean of $S \pm \sigma_0$ for various selections and 100-kyr running mean are shown together with individual results for single points. Magenta marker denotes the $S \pm \sigma_1$ at the LGM ($23 - 19$ ka BP).